Organic LETTERS

Letter

pubs.acs.org/OrgLett

2,5,8,11-Tetraalkenyl Perylene Bisimides: Direct Regioselective Synthesis and Enhanced $\pi-\pi$ Stacking Interaction

Li Zhang,[†] Dezhi He,[†] Yudong Liu,[†] Kun Wang,[‡] Zongxia Guo,[‡] Jianbin Lin,*[,†] and Hui-Jun Zhang*[,†]

[†]Department of Chemistry, College of Chemistry and Chemical Engineering, Xiamen University, Xiamen 361005, People's Republic of China

[‡]School of Polymer Science and Engineering, Qingdao University of Science and Technology, Qingdao 266042, People's Republic of China

Supporting Information

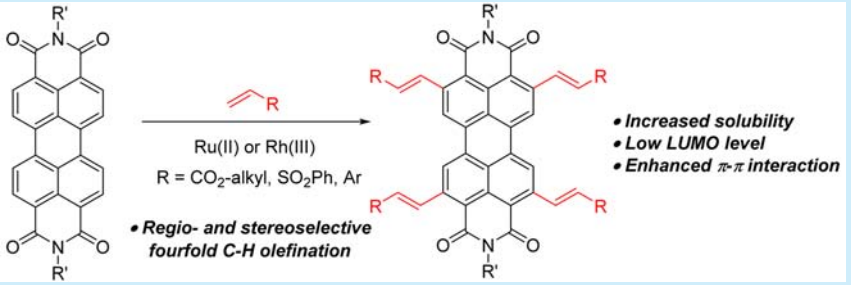

ABSTRACT: A series of 2,5,8,11-tetraalkenyl perylene bisimide (PBI) derivatives were synthesized through Ru(II)- or Rh(III)-catalyzed regio- and steroselective oxidative C−H olefination in one step. The optical electronic and self-assembly of the 2,5,8,11-substituted PBIs were investigated, which showed great potential in optoelectronic applications.

Perylene bisimide (PBI) derivatives, which have high electron affinity and excellent transport property, are promising candidates for applications in (opto)electronics devices.[1] Recently, more and more attention has been focused on the modification of PBI structure to modulate their chemical and physical properties. For example, the introduction of branched or bulky solubilizing groups at the imidic nitrogen is frequently employed to improve their solubility in common organic solvents, which allows for them to be processed into organic electronic devices. And the functionalization at the 1,6,7,12-positions (*bay*-positions) of PBIs is also considered to increase the solubility and modulate the photophysical and redox properties. However, the steric hindrance of branched groups and the *bay*-substituent-dependent core distortion interrupt the $\pi-\pi$ stacking of PBIs, which presumably is detrimental to the electron mobility. More importantly, the efficient $\pi-\pi$ stacking interactions between PBIs is critical for self-assembly into extended nanostructures, which has a strong effect on device performance.[2] For example, 1D nanostructures of PBIs driven by $\pi-\pi$ stacking exhibit uniaxial optical and electronic properties along the 1D $\pi-\pi$ stacking direction.[3] Hence, strategies to functionalize PBIs with enhanced $\pi-\pi$ stacking interaction are desirable.[4]

In comparison with the *bay*-functionalized-PBIs, the selective *ortho*-substituted-PBIs holds more promise as functional materials by virtue of the favorable balance between the $\pi-\pi$ stacking, energy levels and solubility.[3b] However, due to the highly electron-deficient property of the PBI core and higher reactivity of the *bay* positions toward electrophilic substitution,[5] regioselective functionalization at the *ortho* positions is a challenging task. Until recently, several synthetic procedures based on transition-metal-catalyzed *ortho*-C−H functionalization of PBIs have been reported.[6] Treatment of PBIs with alkenes, arylboronates, and bis(pinacolato)diboron, respectively, in the presence of the Murai catalyst ($RuH_2(CO)(PPh_3)_3$) afforded the corresponding 2,5,8,11-alkylation,[6a,7] -arylation,[8] and -borylation products.[9] Through the introduction of these *ortho*-substituents, the solubility and the LUMO level[8,9] of the new PBI derivatives have been proven to be well tailored without causing geometric distortion of the PBI core. However, these synthetic methodologies still have some limitations such as the narrow substrate scope and the low functional group tolerance of the Murai catalyst.[6c] Therefore, other efficient and facile methodologies for the synthesis of new *ortho*-substituted PBIs should be developed to explore desirable functional properties.

Introducing alkene as conjugating bridges at the *ortho*-positions of PBIs presents major advantages as follows: (1) extended π-conjugation may facilitate efficient π-electron delocalization and intermolecular $\pi-\pi$ stacking; (2) incorporation of electron-withdrawing/-donating segments may influence the LUMO level and increase the solubility of PBIs. Recently, Glorius and co-workers achieved the rhodium-catalyzed oxidative olefination of acetophenones and benzamides through twofold C−H functionalization.[10,11] Later,

Received: October 6, 2016
Published: November 10, 2016

DOI: 10.1021/acs.orglett.6b03012
Org. Lett. 2016, 18, 5908−5911

similar carbonyl-directed Heck-type C−H olefinatin catalyzed by less-expensive ruthenium complex $[RuCl_2(p\text{-cymene})]_2$ received more attention.[12] Encouraged by this seminal work, we decided to explore the regioselective direct 2,5,8,11-olefination of PBIs under ruthenium or rhodium catalysis.

Initially, PBI **1a** containing branched side chains and methyl acrylate were chosen as model substrates. After a careful screening of reaction conditions (see the Supporting Information Table S1), we found that treatment of PBI **1a** with methyl acrylate in the presence of 20 mol % of $[RuCl_2(p\text{-cymene})]_2$, 80 mol % $AgSbF_6$, 10 equiv of $Cu(OAc)_2{\cdot}H_2O$, and 4 equiv of HOAc in 1,2-dichloroethane (DCE) at 120 °C for 96 h afforded the 2,5,8,11-tetraolefination product **2a** in 77% yield (Scheme 1) with excellent *E*-stereoselectivity. Thereafter, it was

Scheme 1. Ru(II)- or Rh(III)-Catalyzed Selective Oxidative C−H Alkenylation of PBIs

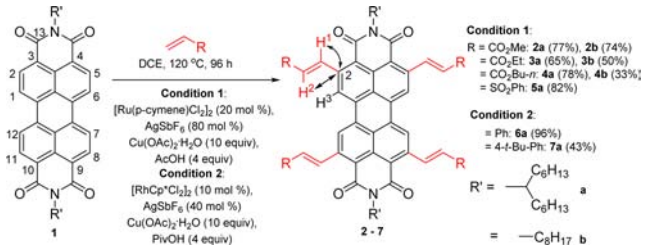

found that the reactions of **1a** with other activated alkenes bearing $-CO_2R$ (R = Et, Bu) and $-SO_2Ph$ groups under the same reaction conditions all proceeded with good yields (**3a**, 65%; **4a**, 78%; **5a**, 82%). Then, the reaction of PBI **1b** containing liner side chains with methyl acrylate was also performed, which gave the desired product **2b** in 74% yield. The tetraolefination of PBI **1b** with ethyl acrylate and butyl acrylate, respectively, gave the corresponding **3b** and **4b** in relatively lower yields (50% and 33%) perhaps due to the lower solubility of PBI **1b** compared with PBI **1a** in DCE. Subsequently, more active rhodium catalyst $[RhCp^*Cl_2]_2$ was employed instead of the ruthenium catalyst to achieve the 2,5,8,11-tetraolefination of **1a** with styrenes (see Table S2). The corresponding *ortho*-tetraalkenyl PBIs **6**−**7a** were obtained in good yields (**6a**, 96%; **7a**, 43%).

The configuration of the tetraalkenylated PBIs was evidenced by NMR spectroscopy. First, the ^{13}C NMR spectra of compounds **2**−**7a** suggested that two very similar isomers in a 1:1 ratio are present due to restricted rotation of the bulky 1-hexylheptyl group around the N−C bond.[13] According to the previous report,[14] the three doubled signals of **2a** represent the carbons that are closest to the restricted N−C bond: C^{13}, C^2, C^3 respectively (Scheme 1). Thereafter, the HMBC experiment was conducted. The correlations between C^2 and H^1 (H^2) indicated the selective formation of *ortho*-substituted-PBIs (Figure S1). Finally, the excellent *E*-stereoselectivity was confirmed by a single set of ^1H NMR signals and the large NMR coupling constants ($J_{H^1-H^2}$ = 15.9−16.0 Hz).

All these *ortho*-tetraalkenyl PBIs showed enhanced solubility in common organic solvents, such as dichloromethane (DCM), $CHCl_3$, and THF, which makes them potential candidates for solution processable electronic devices.

Thereafter, the molecular conformations of PBIs in solution were investigated. The extremely low-field signals for H^1 in the ^1H NMR spectra of all *ortho*-tetraalkenyl PBIs (at approximately 8.8 ppm for H^1 vs 6.5 ppm for H^2) show the possibility of a C−H···O H-bond in $CHCl_3$.[15] The optophysical properties of compounds **1**−**7a** were studied by UV−visible and photoluminescence spectroscopy. All these compounds displayed an absorption band between 400 and 550 nm. The fluorescence spectra were mirror images of the corresponding absorption bands. Compared to the compound **1a**, a red shift in the absorption (7 nm) and emission (10 nm) was observed for the derivatives **2**−**5a**. However, the fluorescence of **6a** and **7a** were most strongly quenched (Figure 1 and Figure S2−S3). The decrease in the fluorescence quantum yields of PBI **2**−**5a** was also observed (Table 1).

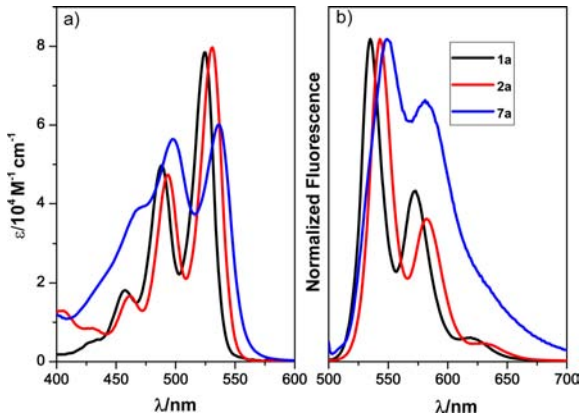

Figure 1. (a) UV−visible absorption spectra and (b) fluorescence spectra (λ_{exc} = 490 nm) of compound **1a**, **2a**, **7a** in DCM (10 μM).

Table 1. Electronic and Optical Properties of PBIs 1−7a

PBIs	E_{red1} [V][a]	E_{red2} [V][a]	E_g [eV][b]	LUMO [eV][c]	HOMO [eV][d]	φ_f[e]
1a	−1.16	−1.37	2.29	−3.64	−5.93	0.89
2a	−0.96	−1.20	2.23	−3.84	−6.07	0.41
3a	−0.98	−1.21	2.23	−3.82	−6.05	0.43
4a	−0.97	−1.20	2.23	−3.83	−6.06	0.62
5a	−0.85	−1.13	2.24	−3.95	−6.19	0.39
6a	−1.19	−1.37	2.21	−3.61	−5.82	–
7a	−1.21	−1.38	2.21	−3.59	−5.80	–

[a]Determined by cyclic voltammetric measurement in 0.1 M solution of Bu_4NPF_6 in DCM: vs Fc/Fc^+. [b]E_g = optical gap, calculated from the optical absorption data. [c]Estimated vs vacuum level from LUMO = 4.80 eV − E_{red1}. [d]Estimated from HOMO = LUMO − E_g. [e]Absolute quantum yield determined by a calibrated integrating sphere system in DCM solution.

Subsequently, the electrochemical properties of PBI derivatives were characterized by cyclic voltammetry in DCM containing 0.1 M Bu_4NPF_6 as a supporting electrolyte. Cyclic voltammetric analysis showed two reversible reduction waves corresponding to the formation of the radical anions and dianions for compounds **1**−**7a** (Figure S4). The calculated HOMO and LUMO values are shown in Table 1. The LUMO levels of compounds **2**−**5a** were comparable to the known halo-substituted PBI derivatives due to the electron-withdrawing acrylate groups.[9] In comparison, the LUMO energy of phenyl-substituted PBI **6**−**7a** was slightly lower.

Recently, Wasielewski and co-workers reported that *ortho*-substituted-PBIs with *n*-octyl chains at imide nitrogen positions form face-to-face slip-stacking.[16] However, the *ortho*-substituted-PBIs with branched imide substituents[17] showed weak intermolecular interaction due to the steric hindrance.[18] The

DOI: 10.1021/acs.orglett.6b03012
Org. Lett. 2016, 18, 5908−5911

branched imide substituted compounds **2**−**4a** with the relatively higher solubility and lower LUMO levels encouraged us to further focus on their $\pi-\pi$ stacking abilities. The absorption and fluorescence spectra of compounds **1**−**4a** in good solvent-DCM are virtually identical (Figure 1). When dispersed in poor solvent-methanol, compounds **2**−**4a** undergo aggregations, and a new band emerges around 565 nm. Moreover, the transitions from ground state to the higher levels of electronic states are enhanced compared to the 0−0 transition (Figure 2a). Such a spectral change implies strong

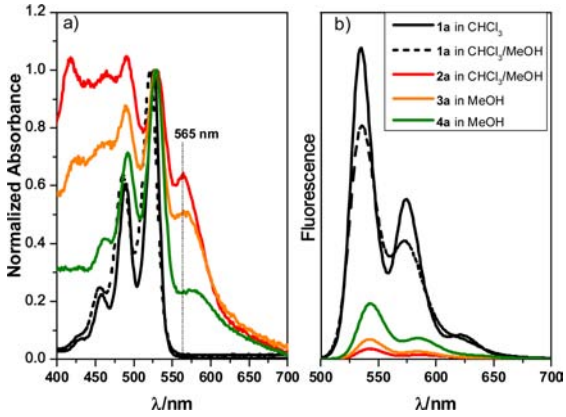

Figure 2. (a) UV−vis absorption spectra and (b) fluorescence spectra (λ_{exc} = 490 nm) of **1**−**4a** (**1a**, **2a** 5 μM in (50 μL of $CHCl_3$ + 1950 μL of MeOH), **3a**, **4a** 5 μM in MeOH, the absorption spectra are normalized at the 0−0 transition maximum).

molecular stacking between the PBI molecules. This is further supported by the fact that the fluorescence of **2**−**4a** was significantly quenched due to the $\pi-\pi$ electronic coupling (Figure 2b).[2b,19] In contrast, for the molecule **1a**, under the same conditions, no new absorption at longer wavelength was observed and no emission was quenched, which imply the weak $\pi-\pi$ interaction of **1a** owing to the steric hindrance of the branched side chains. The $\pi-\pi$ stacking in the solid state was also evidenced by the absorption spectrum of a thin film prepared from a high concentration solution of **2a** in $CHCl_3$/MeOH (Figure S5).

Concentration-dependent UV−visible spectra of **3a**[20] in ethanol were also recorded. At low concentration, absorption spectra of molecularly dissolved **3a** was observed. Upon increasing the concentration, a broadening of the absorption band with concomitant decrease of the absorption coefficients and arising of a new band at longer wavelength around 565 nm, provided evidence for the aggregation of **3a** at high concentration (Figure 3a).[21] The temperature dependent UV−visible spectroscopy of **3a** in ethanol also clearly indicated that, at lower temperatures, the absorption intensity of monomer decreased while that of the aggregate (565 nm) increased. At higher temperatures, more single molecules were dissociated from the aggregate (Figure 3b). An isosbestic point at 550 nm suggested the transformation between the aggregates and single molecules.

The energy-minimized conformation of molecular stacking determines the morphology of the molecular aggregate. To investigate the *ortho*-substitution effect on the PBI aggregate morphology, the aggregate suspension on a silicon oxide film through drop-coating (0.25 mM in 1/1 $CHCl_3$/MeOH) was characterized by field emission scanning electron microscopy

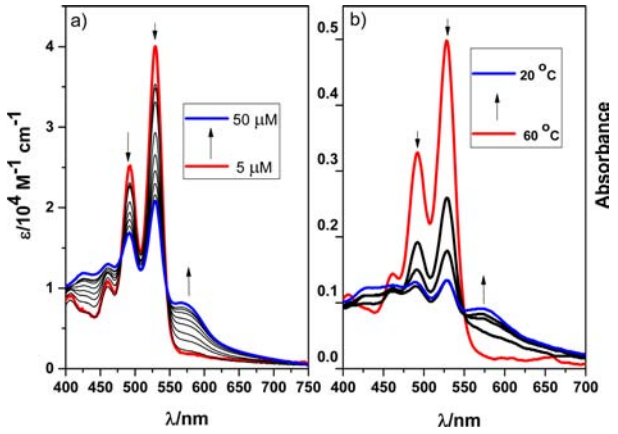

Figure 3. (a) Concentration- and (b) temperature-dependent UV−visible spectroscopy of **3a** in ethanol. The arrows indicate the spectral changes upon (a) increasing concentrations and (b) lowering temperature (10 μM).

(FESEM). As previously reported, the FESEM image of **1a** with branched tails showed a particulate aggregate in an approximately 0D spherical shape with an average size of about 2 μm (Figure 4a).[19] In contrast, the favorable $\pi-\pi$ stacking of **2**−**4a**

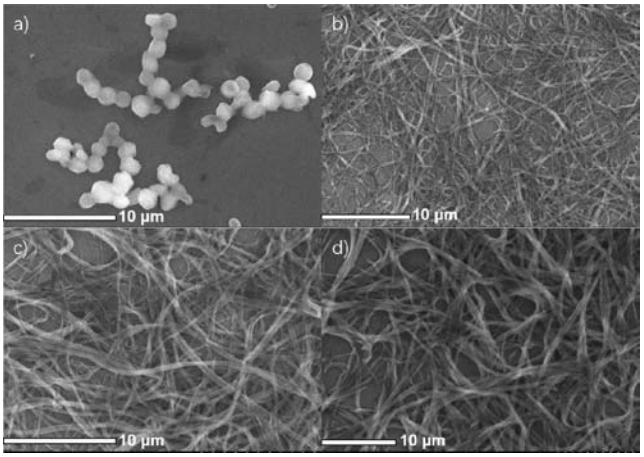

Figure 4. FESEM images of the (a) **1a**, (b) **2a**, (c) **3a**, (d) **4a** (prepared by drop-coating one drop 0.25 mM $CHCl_3$/MeOH (1/1) suspension on a silicon oxide film).

led to the formation of 1D molecular assembly nanobelts. Their average widths were about 300, 400, and 600 nm respectively with typical lengths in the range of several tens of microns (Figure 4b−d). The large aspect ratios (length over width) of these nanobelts revealed the totally different molecular packing modes of **2**−**4a** from **1a**.[19] Detailed nanostructure information on individual nanobelts was also obtained through AFM studies. The AFM observation revealed that the relatively uniform nanobelts with large aspect ratios were consistent with the SEM observation (Figure S6).

In conclusion, an efficient and facile methodology for the synthesis of 2,5,8,11-tetraalkenyl-PBIs has been developed through Ru(II)- or Rh(III)-catalyzed selective oxidative C−H olefination. Compared with the unsubstituted parent PBIs, the introduction of *ortho*-tetraalkenyl groups not only increased the solubilities but also lowered their LUMO levels. Interestingly, the packing models were changed from 0D to 1D due to the enhanced $\pi-\pi$ stacking interactions between 2,5,8,11-tetraal-

DOI: 10.1021/acs.orglett.6b03012
Org. Lett. 2016, 18, 5908−5911

kenyl-PBIs. The facile synthesis and unique properties of these *ortho*-tetraalkenyl-PBIs set up a new way for us to explore novel PBI-based materials, which are promising candidates for organic electronics and optoelectronics devices.

■ ASSOCIATED CONTENT

Supporting Information

The Supporting Information is available free of charge on the ACS Publications website at DOI: 10.1021/acs.orglett.6b03012.

Reaction condition screening tables, experimental procedures, full characterization data (PDF)

■ AUTHOR INFORMATION

Corresponding Authors

*E-mail: jb.lin@xmu.edu.cn.
*E-mail: meghjzhang@xmu.edu.cn.

ORCID

Jianbin Lin: 0000-0002-0064-3079

Notes

The authors declare no competing financial interest.

■ ACKNOWLEDGMENTS

We are grateful for financial support from the Natural Science Foundation of China (No. 21302157, 21302159, 21572188, 21573118) and Fundamental Research Funds for the Central Universities (No. 20720160049, 20720140536). We also thank Albert Schenning (The Eindhoven University of Technology) for useful discussions.

■ REFERENCES

(1) (a) Würthner, F.; Saha-Möller, C. R.; Fimmel, B.; Ogi, S.; Leowanawat, P.; Schmidt, D. *Chem. Rev.* **2016**, *116*, 962−1052. (b) Würthner, F. *Chem. Commun.* **2004**, 1564−1579.

(2) (a) Struijk, C. W.; Sieval, A. B.; Dakhorst, J. E.; van Dijk, M.; Kimkes, P.; Koehorst, R. B.; Donker, H.; Schaafsma, T. J.; Picken, S. J.; van de Craats, A. M. *J. Am. Chem. Soc.* **2000**, *122*, 11057−11066. (b) Seki, T.; Maruya, Y.; Nakayama, K.; Karatsu, T.; Kitamura, A.; Yagai, S. *Chem. Commun.* **2011**, *47*, 12447−12449.

(3) (a) Würthner, F.; Stolte, M. *Chem. Commun.* **2011**, *47*, 5109−5115. (b) Chen, S.; Slattum, P.; Wang, C.; Zang, L. *Chem. Rev.* **2015**, *115*, 11967−11998.

(4) (a) Zhao, D.; Wu, Q.; Cai, Z.; Zheng, T.; Chen, W.; Lu, J.; Yu, L. *Chem. Mater.* **2016**, *28*, 1139−1146. (b) Wu, Q.; Zhao, D.; Schneider, A. M.; Chen, W.; Yu, L. *J. Am. Chem. Soc.* **2016**, *138*, 7248−7251.

(5) Yue, W.; Li, Y.; Jiang, W.; Zhen, Y.; Wang, Z. *Org. Lett.* **2009**, *11*, 5430−5433.

(6) (a) Nakazono, S.; Imazaki, Y.; Yoo, H.; Yang, J.; Sasamori, T.; Tokitoh, N.; Cédric, T.; Kageyama, H.; Kim, D.; Shinokubo, H.; Osuka, A. *Chem. - Eur. J.* **2009**, *15*, 7530−7533. (b) Teraoka, T.; Hiroto, S.; Shinokubo, H. *Org. Lett.* **2011**, *13*, 2532−2535. (c) Battagliarin, G.; Li, C.; Enkelmann, V.; Mullen, K. *Org. Lett.* **2011**, *13*, 3012−3015.

(7) Dasgupta, D.; Kendhale, A. M.; Debije, M. G.; ter Schiphorst, J.; Shishmanova, I.; Portale, G.; Schenning, A. P. *ChemistryOpen* **2014**, *3*, 138−141.

(8) Nakazono, S.; Easwaramoorthi, S.; Kim, D.; Shinokubo, H.; Osuka, A. *Org. Lett.* **2009**, *11*, 5426−5429.

(9) Battagliarin, G.; Zhao, Y.; Li, C.; Müllen, K. *Org. Lett.* **2011**, *13*, 3399−3401.

(10) Patureau, F. W.; Besset, T.; Glorius, F. *Angew. Chem., Int. Ed.* **2011**, *50*, 1064−1067.

(11) For recent reviews that feature C−H olefinations, see: (a) Zhou, L.; Lu, W. *Chem. - Eur. J.* **2014**, *20*, 634−642. (b) Kozhushkov, S. I.; Ackermann, L. *Chem. Sci.* **2013**, *4*, 886−896. (c) Arockiam, P. B.; Bruneau, C.; Dixneuf, P. H. *Chem. Rev.* **2012**, *112*, 5879−5918. (d) Patureau, F. W.; Wencel-Delord, J.; Glorius, F. *Aldrichimica Acta* **2012**, *45*, 31−41. (e) Le Bras, J.; Muzart, J. *Chem. Rev.* **2011**, *111*, 1170−1214. (f) Satoh, T.; Miura, M. *Chem. - Eur. J.* **2010**, *16*, 11212−11222.

(12) Padala, K.; Jeganmohan, M. *Org. Lett.* **2011**, *13*, 6144−6147.

(13) At 323 K, the ^{13}C NMR spectrum simplified, with the three sets of doubled peaks becoming singlets. See SI.

(14) Wescott, L. D.; Mattern, D. L. *J. Org. Chem.* **2003**, *68*, 10058−10066.

(15) (a) Desiraju, G. R. *Acc. Chem. Res.* **1996**, *29*, 441−449. (b) Langhals, H.; Schönmann, G.; Polborn, K. *Chem. - Eur. J.* **2008**, *14*, 5290−5303.

(16) (a) Eaton, S. W.; Shoer, L. E.; Karlen, S. D.; Dyar, S. M.; Margulies, E. A.; Veldkamp, B. S.; Ramanan, C.; Hartzler, D. A.; Savikhin, S.; Marks, T. J.; Wasielewski, M. R. *J. Am. Chem. Soc.* **2013**, *135*, 14701−14712. (b) Hartnett, P. E.; Timalsina, A.; Matte, H. S. S. R.; Zhou, N.; Guo, X.; Zhao, W.; Facchetti, A.; Chang, R. P. H.; Hersam, M. C.; Wasielewski, M. R.; Marks, T. J. *J. Am. Chem. Soc.* **2014**, *136*, 16345−16356.

(17) Yu, Z.; Wu, Y.; Liao, Q.; Zhang, H.; Bai, S.; Li, H.; Xu, Z.; Sun, C.; Wang, X.; Yao, J.; Fu, H. *J. Am. Chem. Soc.* **2015**, *137*, 15105−15111.

(18) Zang, L.; Che, Y.; Moore, J. S. *Acc. Chem. Res.* **2008**, *41*, 1596−1608.

(19) Balakrishnan, K.; Datar, A.; Naddo, T.; Huang, J.; Oitker, R.; Yen, M.; Zhao, J.; Zang, L. *J. Am. Chem. Soc.* **2006**, *128*, 7390−7398.

(20) Due to the limited solubility in alcohol, **3a** in ethanol was chosen for the temperature-dependent UV−visible spectroscopy study, and tiny amounts of $CHCl_3$ were used to increase the solubility in the concentration-dependent UV−visible spectroscopy study.

(21) Chen, Z.; Fimmel, B.; Würthner, F. *Org. Biomol. Chem.* **2012**, *10*, 5845−5855.

DOI: 10.1021/acs.orglett.6b03012
Org. Lett. 2016, 18, 5908−5911